

# Frozen mode in coupled single-mode waveguides with gratings

Albert Herrero-Parareda , Nathaniel Furman , Bradley J. Thompson, , Ricky Gibson, , Ilya Vitebskiy, ,  
and Filippo Capolino 

**Abstract**—We present a systematic methodology for designing slow-light photonic integrated circuits with a frozen mode based on a special kind of exceptional point of degeneracy (EPD) of order three named stationary inflection points (SIPs). This is realized through three-way coupled waveguides with lateral gratings operating at telecommunication wavelengths. We provide two designs and analyze sensitivity to geometric perturbations. We have fabricated a periodic waveguide with integrated taper loads and demonstrate reasonable agreement with full-wave simulations. These findings confirm the feasibility of integrating SIP-based delay functionalities in standard silicon photonic platforms.

## I. INTRODUCTION

The growth of increasingly precise nanometric fabrication practices leads to the development of photonic integrated circuits (PICs) wherein integrated optical devices such as waveguides and resonators are built within a common semiconductor wafer.

Here, we focus on a new design of gainless and lossless PIC waveguides that support an exceptional point of degeneracy (EPD) that is a point in the parameter space of a system where the eigenstates coalesce. Some early studies of guiding systems supporting this kind of EPDs are Refs. [1], [2], [3], where the authors discuss the physical aspects of the same EPD studied here using the term "stationary point" without resorting to the term exceptional point. In particular, in this paper we focus on the stationary inflection point (SIP) that is an EPD of order three. EPDs feature in a variety of classical and quantum mechanical problems [4], most notoriously in the presence of balanced gain and loss (a condition known as PT-symmetry [5], [6], [7]).

EPDs in periodic photonic devices can be achieved through dispersion engineering without the need for gain or loss [8]. The concept was earlier explored in Refs. [9], [10], [3], [11], [12] without using the term "exceptional point". Other examples of dispersion diagrams that show a stationary inflection point are Refs. [13], [14], [15], [16], though not relating it to stationary points or EPDs. The order of the EPD is given by the number of coalescing eigenmodes, and it is very important in determining the properties of the finite-length device. Devices operating near EPDs also display a heightened sensitivity to parameter perturbations, which is part of the reason why the successful fabrication of high-order EPD-based PICs has been

difficult to achieve. Only a handful of experimental studies exist in optics, as in [17] for the degenerate band edge and in [18] for the SIP.

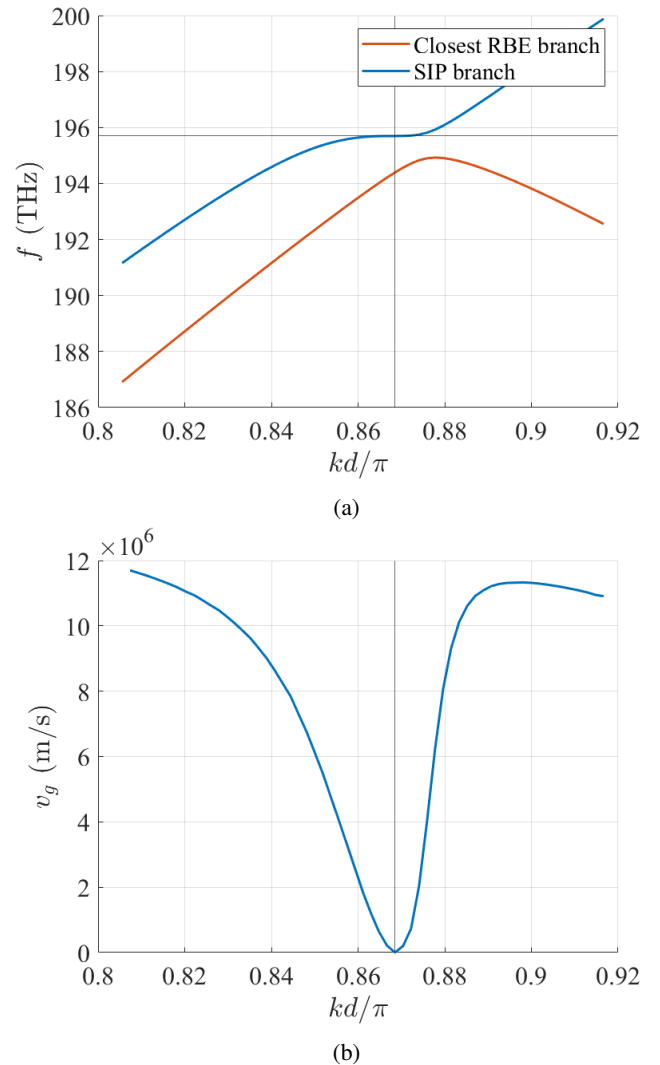


Fig. 1: (a) Modal dispersion diagram of the SIP-supporting mode of the TWG2RA (in blue) and the closest RBE mode (in orange); and (b) group velocity  $v_g$  against Bloch wavenumber around the SIP.

A. Herrero-Parareda, N. Furman, and F. Capolino are affiliated with the Department of Electrical Engineering and Computer Science, University of California, Irvine, CA, 92697 USA. B. J. Thompson, R. Gibson, and I. Vitebskiy are affiliated with Air Force Research Laboratory, Sensors Directorate, Wright-Patterson AFB, OH, 45433 USA. e-mail: f.capolino@uci.edu.

extremely low group velocity ( $v_g = \partial\omega/\partial k$ ) and enhanced field amplitudes away from the cavity's edge. At the edges of the device, propagating and evanescent modes interfere destructively, satisfying the boundary conditions [3] and creating unique field properties and field enhancement. An EPD of order 2 is a regular band edge (RBE) involving only two counter-propagating modes which results in a standard standing wave [8]. Higher order EPDs instead involve evanescent fields as well [9], [10], [8]. The lowest-order EPD to display the frozen mode is known as a stationary inflection point (SIP); it is identified as an inflection point in the Bloch mode dispersion diagram of the waveguide, and it is an EPD of order three [8], [19].

Figure 1(a) shows the real branches of the modal dispersion diagram of an SIP-supporting design and (b) shows its group velocity  $v_g = 2\pi\partial f/\partial k$  against the Bloch wavenumber  $k$  near the SIP. The group velocity reaches a minimum at the SIP wavenumber  $k_S$ . Though not shown in Fig. 1 because only the propagation branches are shown, there are three modes coalescing at the SIP when considering also the evanescent modes. The frozen mode associated with the stationary inflection point that is an EPD of order 3 cannot be generated with only two counter-propagating modes because evanescent modes are also needed. Therefore, at least three modes (propagating or evanescent) in each direction, properly coupled, are needed, as explained in [3], [12], [8], [19].

Operating near an SIP offers advantages over an RBE: it supports the frozen mode while exhibiting lower sensitivity than higher-order EPDs, and it is not sided by a band gap. Therefore, even though the SIP displays an asymmetric group velocity dispersion (the group velocity variation with frequency), signal distortion can be undone as long as the transmission spectrum of the waveguide is properly characterized. For its unique dispersion, the SIP has been proposed as a strategy to conceive devices that reach large true time delay [20], [21]. It is also investigated to conceive new lasing regimes [22], [23], [24], [25], and nonlinear isolators, because of its unique properties.

We introduce a method for designing periodic PIC waveguides that support an SIP through dispersion engineering. The resulting structures, referred to as three-way coupled waveguides, consist of either two gratings coupled to a central waveguide (TWG2) or a single grating side-coupled to two adjacent straight waveguides (TWG1). The SIP arises from the synchronization of three modes: one propagating and two evanescent, which coalesce into a frozen mode. To achieve this, we develop and analyze three designs (two TWG1s and one TWG2), shown respectively in Fig. 2(a) and (b), and design their geometries to account for realistic waveguide cross-sections and fabrication tolerances, using eigenmode-based analysis. To the best of the authors' knowledge, SIP waveguides using these PIC compatible waveguides with lateral gratings have never been shown before. Furthermore, we show that the proposed structures exhibit some resilience to simulation-mesh quality and waveguide dimensions. After the waveguide design and tapeout preparation, we measure the transfer function of fabricated devices. We compare the measured spectral response to the same structure in simulation

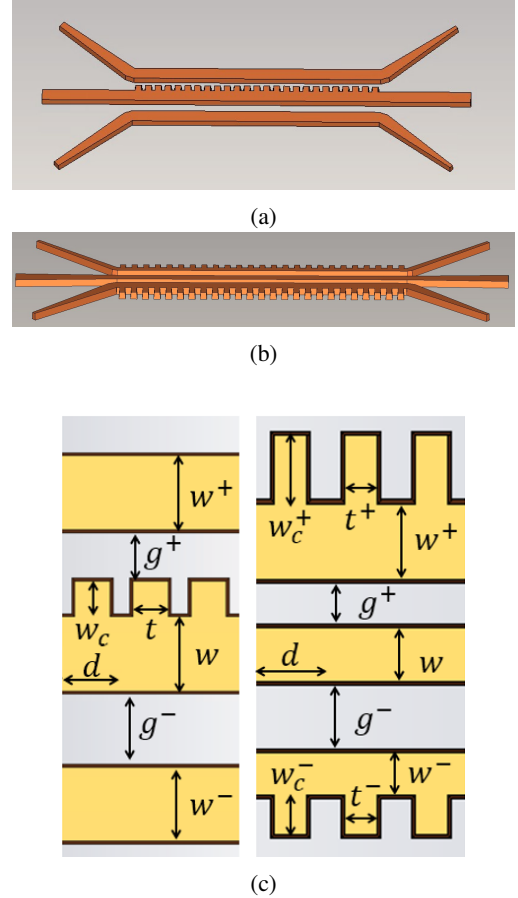


Fig. 2: Schematic representations: (a) TWG1 waveguide with a central grating side-coupled to two straight waveguides; (b) TWG2 waveguide made of a central straight waveguide side-coupled to two grating waveguides; (c) top view of the two TWG1 and TWG2 waveguides showing the unit cells.

and investigate the group delay in simulations.

The paper is organized as follows: The methodology to design SIP-supporting three-way waveguides is described in Section II. In Section III, we highlight the expected differences between design and fabrication, leading to a redesign that is more consistent with fabrication methods. The experimental features of finite-length SIP waveguides are discussed in Section IV. The results are summarized in Section V.

## II. PROCESS STEPS TO DESIGN AN SIP

To design an SIP-supporting PIC, the *first step* is to couple a waveguide with grating to a straight channel waveguide such that their counter-propagating modes that meet near a target point  $(k_S, f_S)$  in the Brillouin zone, form a bandgap around  $f_S$ . A third waveguide with an optical mode is then positioned adjacent to the coupled pair. As it is brought closer, the interaction among the three waveguides generates local extrema in the dispersion near  $f_S$ . Fine parameter tuning enables the formation of an SIP at the desired location.

Figure 3 illustrates the SIP design process using the TWG1 configuration as an example. Panels (a) and (b) show the individual dispersion diagrams of the (a) grating-straight wave-

uide pair, and (b) the individual third waveguide, respectively. In (c), the lightly coupled three-way structure shows local maxima and minima near  $(k_S, f_S)$ . In (d), after optimizing parameters such as waveguide widths and gaps, an SIP is achieved, identified by a stationary inflection in the Bloch dispersion diagram with vanishing group velocity at  $(k_S, f_S)$ . Similar dispersion diagrams are shown in [11] depending on the value of a waveguide parameter.

We designed two TWG2 waveguides and one TWG1 waveguide (TWG2A, TWG2B, and TWG1A) supporting an SIP at  $f_S$  in the range [192, 195] THz. Table I summarizes the parameters for each design. A key figure of merit is the frequency separation  $\Delta f_{SR}$  between the SIP and the nearest RBE, which should be large to ensure stable SIP operation in long waveguides. Generally,  $\Delta f_{SR}$  improves with smaller unit cell periods  $d$ , consistent with the increase in free spectral range  $\Delta f_{FSR} = c/(n_w d)$  [15]. Previous photonic integrated waveguides supporting an SIP displayed an estimated  $\Delta f_{SR}$  (in GHz) of: 344 [20], 60 [8], 31 [19], 80 [23], 306 [26], and 186 [25]. As shown in Table I, the designs presented here achieve significantly larger  $\Delta f_{SR}$  than previous SIP designs, such as the  $\Delta f_{SR} = 1000$  GHz of the TWG2RA discussed later on, owing to their small unit cell periods.

TABLE I: SIP-supporting waveguide designs

Params (nm)	TWG2A	TWG2B	TWG1A
$w$	310	300	450
$w^+$	250	250	480
$w^-$	420	325	477
$g^+$	325	325	200
$g^-$	200	200	291
$w_c^+$	200	200	200
$w_c^-$	380	466	-
$t^+$	200	200	200
$t^-$	200	200	-
$d$	350	370	325
$f_s$ (THz)	192.28	193.13	192.95
$k_s d/\pi$	0.983	0.97	0.87
$\Delta f_{SR}$ (GHz)	540	565	80

Modal dispersion relations were obtained using the full-wave eigenmode solver in CST Studio Suite based on the finite element method. Phase shifted periodic boundaries were applied at two virtual cross-sections spaced by one period,  $d$ . The transverse boundary conditions consist of perfect electric conductor (PEC) walls positioned far from the waveguide core, with sufficient silicon dioxide cladding to ensure the evanescent fields decay before reaching the boundaries. Material dispersion is neglected in the frequency range of interest [27]; the refractive indices of the silicon core  $n_{Si} = 3.478$  and cladding  $n_{SiO_2} = 1.444$  are considered constant with respect to the frequency.

### III. WAFER TAPEOUT PREPARATION

Generally, SIP-based devices display a high sensitivity to geometric perturbations, as it happens in EPD systems in general, [28], [2], [8]. To preserve the frozen mode, the

waveguides are here redesigned to account for fabrication-induced constraints that, even if small, may disrupt mode coalescence. A key limitation in fabrication is the minimum feature size, typically around 100 nm.

A common and predictable issue is waveguide cross-section distortion, where fabricated waveguides taper at the top, resulting in a trapezoidal shape rather than the ideal rectangular cross-section assumed earlier in the design process.

The effects of this variation are illustrated in Figure 4, which displays the dispersion diagram for the SIP-TWG2A waveguide with both cross-section types. Introducing a realistic waveguide sidewall angle (i.e., by decreasing the top dimensions based on tilting all walls by a few degrees  $\theta_\delta$  from the  $90^\circ$ ) alters the mode profile, resulting in weaker waveguide coupling. The waveguides are nominally 220 nm wide and the top width is adjusted to account for the realistic sidewall angle  $\theta_\delta$  [29]. Due to the resilience of the waveguide geometry to perturbations, even the TWG2A waveguide with tilted walls still exhibits a flattened dispersion diagram that results in large group delay. However, the SIP condition is slightly disrupted and must be restored through fine parameter optimization. This is what we do next.

The updated values of the parameters for the redesigns that support an SIP with trapezoidal cross-sections are shown in Table II. These values refer to the bottom dimensions. The hyphens in the TWG1RA column serve to show that there is no second grating in this structure.

Preparing frozen mode PICs for wafer tapeout requires a tolerance analysis to evaluate device performance after fabrication. While some analytic models treat tolerances as variations in the effective index [24], we directly study how perturbations affect the Bloch dispersion and the formation of the SIP.

TABLE II: Realistic SIP-supporting waveguide designs

Params (nm)	TWG2RA	TWG2RB	TWG1RA
$w$	310	300	450
$w^+$	250	250	480
$w^-$	420	325	<b>477</b>
$g^+$	<b>319</b>	325	200
$g^-$	200	200	<b>305</b>
$w_c^+$	200	200	200
$w_c^-$	<b>340</b>	<b>436</b>	-
$t^+$	200	200	200
$t^-$	200	200	-
$d$	<b>355</b>	370	325
$f_s$ (THz)	195.755	197.58	194.16
$k_s d/\pi$	0.867	0.91	0.96
$\Delta f_{SR}$ (GHz)	1000	664.5	127.6

Fabrication tolerances are generally around 2 – 5 nm [29], [24] which are either added or subtracted from the nominal geometric parameters. Figure 5 shows the dispersion diagram of the TWG2RB design. The nominal case, in black, and perturbed cases with  $\Delta = \pm 10$  nm applied collectively to the waveguide widths  $w$ ,  $w^+$ , and  $w^-$  in blue and red, respectively. The  $\Delta$  perturbation in width leads to the formation of near stationary points in the dispersion, known as tilted inflection

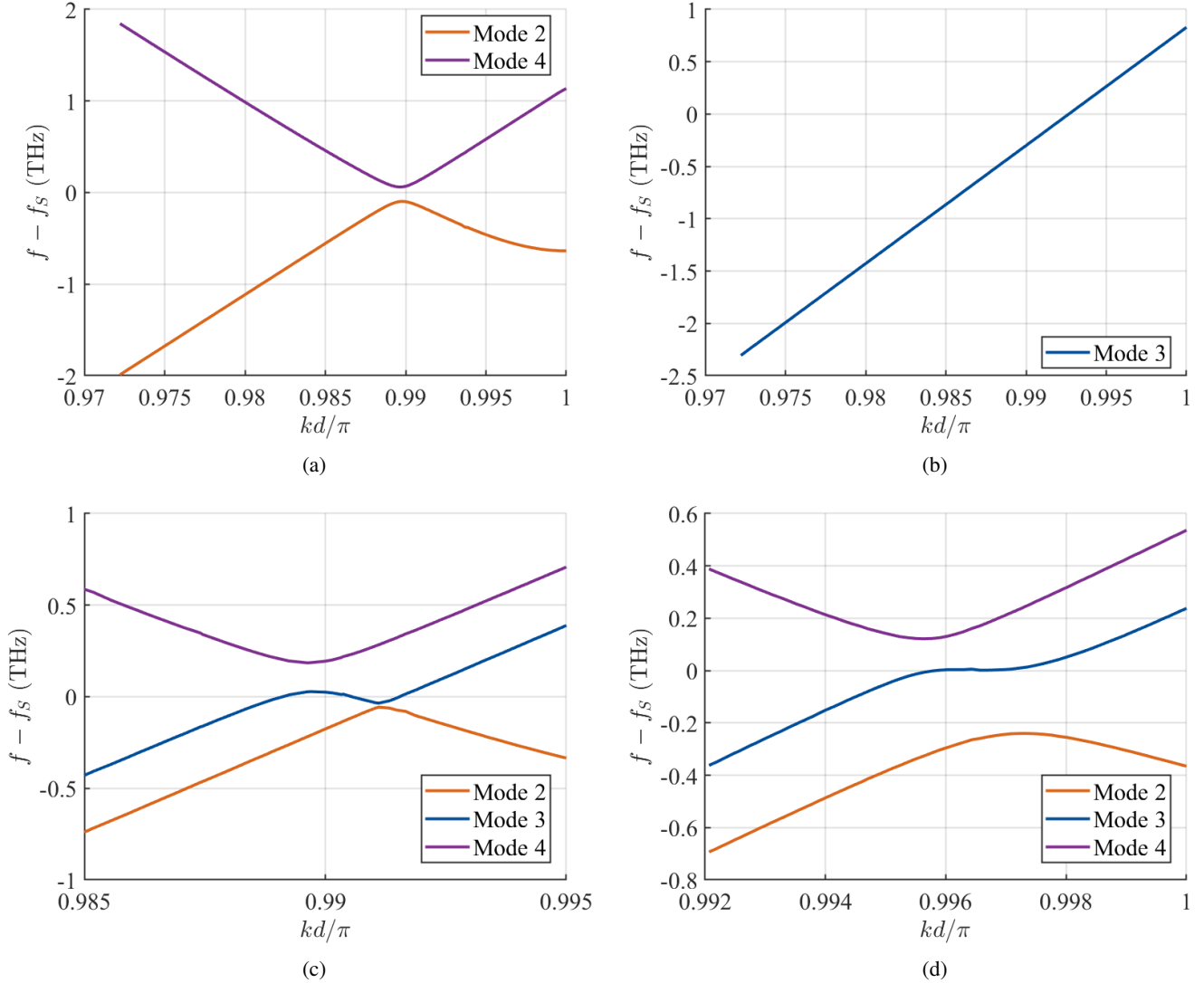


Fig. 3: Design steps for creating a stationary inflection point (SIP)-based frozen mode photonic integrated circuit (PIC) using the TWG1 configuration. (a) Dispersion diagram of a grating coupled to a straight waveguide, with parameters selected to open a bandgap near the target point  $(k_S, f_S)$ . (b) Dispersion diagram of an isolated straight waveguide showing a mode near the same target region. (c) Dispersion diagram of the TWG1 configuration, formed by adding the additional waveguide from (b) to the grating–straight waveguide pair in (a). The resulting structure produces the blue dispersion curve with a local maximum and minimum near the target point  $(k_S, f_S)$ . (d) Optimized TWG1 dispersion diagram after adjusting waveguide gap sizes, where a stationary inflection point (SIP) emerges at the target  $(k_S, f_S)$  location (blue curve).

points (TIPs) [30]. In the example shown in Figure 5, decreasing the parameter values by 10 nm only disrupts the SIP condition slightly. The resulting red curve exhibits a smooth-TIP, a near-inflection point with low but non-zero group velocity. In contrast, increasing the parameter values produces the blue curve, which shows a local maximum and minimum near the SIP frequency. This configuration corresponds to an alternating-TIP, where the group velocity changes sign in the vicinity of the SIP frequency. Such features often appear as intermediate stages in the SIP waveguide design process described in Section II, and in [11] where the authors show the dispersion variation by fine-tuning a waveguide parameter. Comparable asymmetric responses are

observed when varying the corrugation widths, gap sizes, or thicknesses in the TWG2RA (not shown), and in the TWG2RB and TWG1RA designs. These results confirm the resilience of the proposed SIP-based waveguides to some geometric perturbations, as even small changes in waveguide dimensions shift the dispersion notably but the modal dispersions still retain a shape that exhibits inflection points that lead to large group delay. The response is also asymmetric with respect to the direction of the variation, as shown by the different behaviors for  $\Delta = \pm 10\text{nm}$ . In summary, we observe the important result that despite perturbations twice as large as the expected fabrication tolerance (2–5nm), the dispersion still exhibits a strong curvature and low group velocity near the SIP.

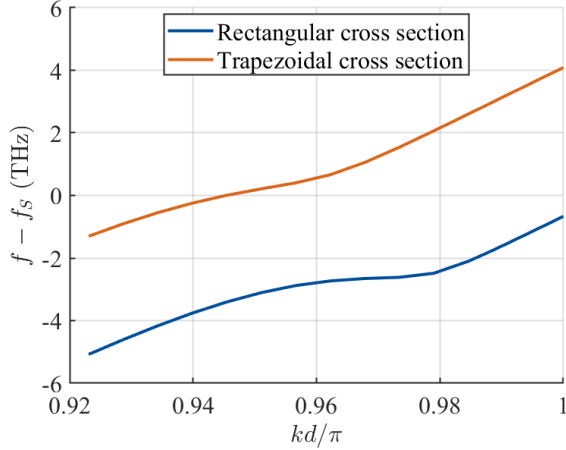


Fig. 4: Dispersion diagram of the SIP-TWG2A waveguide with a rectangular and a trapezoidal cross section. The trapezoidal geometry alters the mode profile. This slightly disrupts the SIP condition, which must be restored through fine tuning of the waveguide parameters.

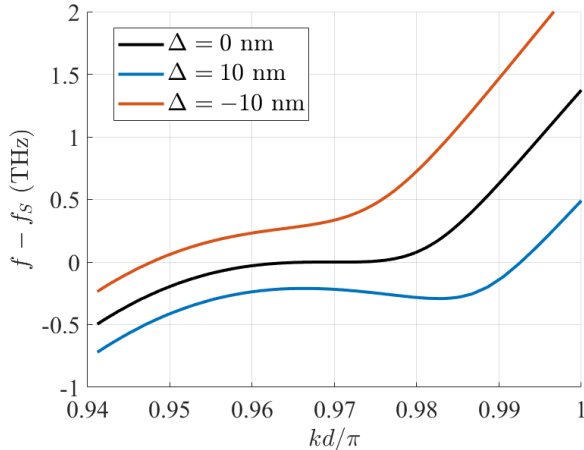


Fig. 5: Dispersion diagram of the TWG2RB design showing the nominal case (black), and variations with waveguide widths increased (blue) and decreased (red) by  $\Delta = 10$  nm. The SIP condition is sensitive to these changes, highlighting the importance of designing for robustness to perturbations.

This indicates that while precise fabrication is critical, the SIP regime remains robust under moderate deviations.

In Figure 6 we show the redesigned waveguide TWG2RA to exhibit an SIP at  $f_s = 195.755$  THz with trapezoidal cross section. We also show the upper and lower branches and their critical points. In particular, the RBE of the blue branch is 1 THz below the SIP of the orange branch. This is the waveguide design that is studied in the next section where we analyze the transfer function and group delay of waveguides with finite length.

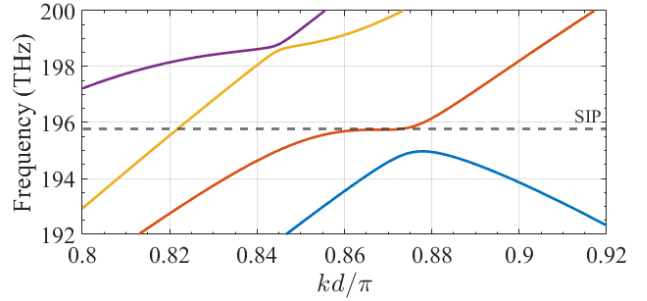


Fig. 6: Dispersion diagram of the SIP-TWG2RA waveguide with a trapezoidal cross section. The three real-wavenumber modes closest to the SIP mode (orange curve) are also shown. The closest RBE is 1 THz lower than the SIP.

#### IV. FINITE-LENGTH SIMULATED AND MEASUREMENT RESULTS

We present finite-length simulation results and extend the discussion of finite-length models to fabricated device measurements of the transfer function. Specifically, the American Institute for Manufacturing Integrated Photonics (AIM Photonics) fabricated these devices on their multi-project wafer (MPW) [29]. We focus on the wafer-ready SIP-TWG2RA design (parameters given in Table II) with  $N = 50$ ,  $N = 100$ , and  $N = 200$  unit cells. The fabricated devices have the same geometry as the simulation where we also consider the sidewall angling. The terminations of the outer two waveguides are angled  $40^\circ$  away from the center waveguide with a taper length of  $4 \mu\text{m}$  and a minimum width of  $200 \text{ nm}$ .

We measured the magnitude of the transfer function of these edge-coupled devices using a high power superluminescent diode (SLD) paired with an optical spectrum analyzer (OSA). The SLD has a spectrum centered around  $\lambda = 1550 \text{ nm}$  ( $\approx 193.4 \text{ THz}$ ) with a significant,  $\approx 20 \text{ dB}$ , signal drop-off at wavelengths smaller than  $\approx 1515 \text{ nm}$  ( $\approx 197.9 \text{ THz}$ ). The simulation data is presented as-is and the measured data is normalized to the SLD spectrum and has its maximum magnitude in the shown frequency range set to  $0 \text{ dB}$ . The SLD/OSA measurement setup well characterizes the spectral response of the devices yet does not have the capability to measure the group delay.

In Fig. 7, we plot the measured data (black curve) and simulation data (red curve) for  $N = 50$ ,  $N = 100$ , and  $N = 200$ . We plot both the transfer function and the group delay (simulation only). Further, to better align the simulation data compared to the measurement, we spectrally shift the black curve by the amount given in the figure legend based on the cross correlation between the simulation and measured data between 196 and  $200 \text{ THz}$ . This frequency shift is comparable to other devices and designs on the same wafer.

We calculate the group delay based on the phase of the transfer function  $\mathcal{L}T_f(\omega)$  as

$$\tau_g = -\frac{\partial \mathcal{L}T_f(\omega)}{\partial \omega}, \quad (1)$$

where  $\omega = 2\pi f = 2\pi c_0/\lambda$  is the angular frequency and  $c_0$

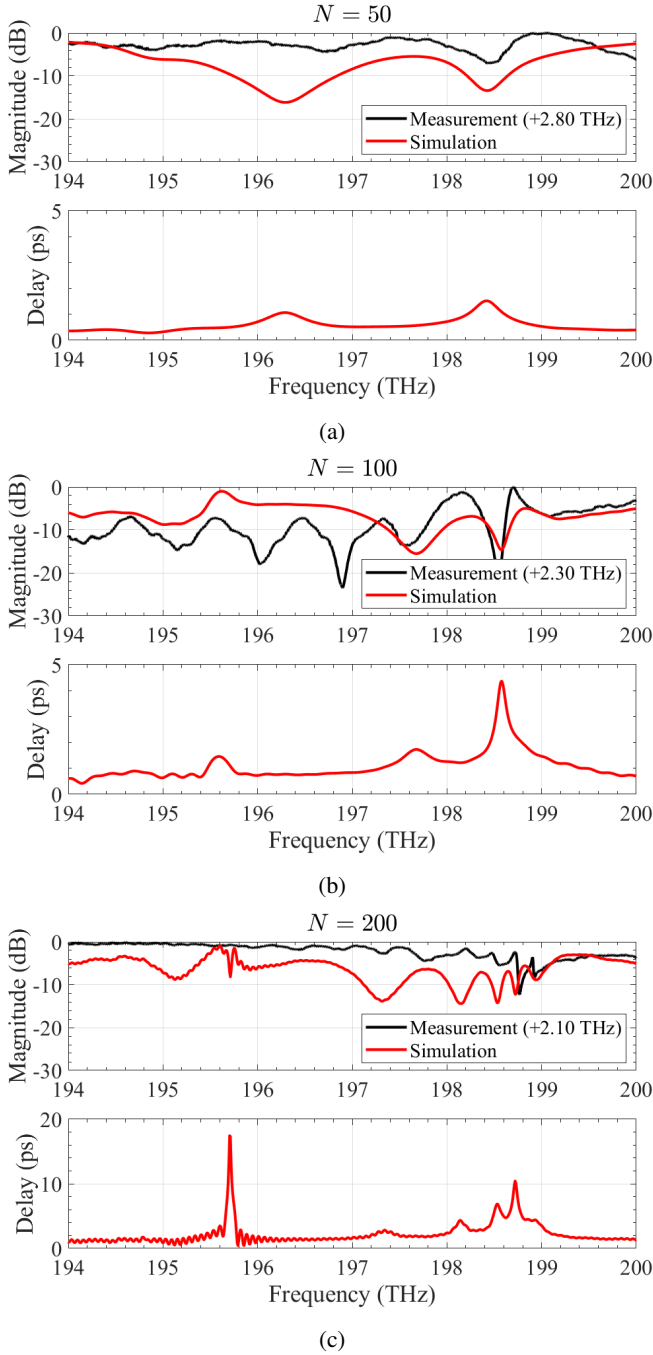


Fig. 7: Transmission profile and group delay for measured and simulated results of the TWG2RA design with (a)  $N = 50$  unit cells, (b)  $N = 100$  unit cells, and (c)  $N = 200$  unit cells. The measurement results are spectrally shifted to better align with simulated results, with their shift displayed in the figure caption. Around the SIP frequency  $f_S = 195.755$  THz, for larger  $N$  we observe a more significant enhancement of the group delay compared to the spectral features around 198.6 THz.

is the speed of light in vacuum. As the phase changes more rapidly over some frequency, we expect to see an increase in the group delay.

Given a waveguide width of  $w = 480$  nm with the modal index calculated from simulations of  $n_w = 2.378$ , the delay per length in a straight uniform waveguide of this width is  $\approx 7.9$  fs/ $\mu\text{m}$ . Using the period of  $d = 355$  nm from Table II, the total length of the  $N = 50$ ,  $N = 100$  and  $N = 200$  devices are 17.75  $\mu\text{m}$ , 35.50  $\mu\text{m}$ , and 71.0  $\mu\text{m}$ , respectively. This corresponds to a total delay in an equivalent straight waveguide of the same length with  $w = 480$  nm of 0.140 ps, 0.280 ps, and 0.560 ps. From simulations, we see delays significantly larger than these values around features of interest. In particular, around the SIP frequency, we observe a very significant increase in delay for  $N = 200$ . For this length, the group delay is 18 ps that is  $\approx 32$  times larger than the 0.560 ps delay of a uniform straight waveguide of the same length. While this delay peak is also seen for  $N = 100$ , for this length the delay peak at nearby spectral features at 198.6 THz is more significant. Only when  $N$  becomes sufficiently large, as for  $N = 200$ , do we observe the delay around the SIP to be quite large and even dominate with respect to that at higher frequencies (compare the scale of the group delay in Fig. 1(b) with that in (d)). This trend of scaling delay with length is also consistent with related SIP-supporting geometries and simulations [31].

Accordingly, for small  $N$  and moderately large  $N$  like 200, it is difficult to definitively determine the asymptotic trends of the group delay with the number of unit cells associated with the SIP or with other flattening regions and band edge degeneracies. Observation of the purple and yellow curves in Fig. 6 shows a flattening of the dispersion and a multi-mode interaction around these higher frequencies which may be related to the moderate growth delays seen here around 198.6 THz. Conversely, as  $N$  increases, the SIP-associated delay increases are more readily observed due to the difference in scaling trends of the SIP compared to other spectrally flattened regions.

## V. CONCLUSION

We have introduced a robust design methodology to obtain three-way coupled waveguides that support an SIP at communication frequencies. The process enables tuning the dispersion diagram to support an SIP at targeted frequencies while accounting for fabrication limitations, such as non-ideal cross-sections and tolerances. Using this approach, we developed and fabricated SIP-supporting waveguides. The agreement between the experiment and simulation results confirms that the fabricated structure closely resembles the fabrication-ready design, which has been numerically shown to support an SIP. A key result is the comparison of measured and simulated transmission profiles in a device with 50, 100, and 200 unit cells. These results show an initial agreement between simulation and measurement with differences comparable to similar studies on the same wafer. Additionally, the group delay from simulation, at a frequency close to the SIP, is significantly larger than that of a standard SOI waveguide of the same length.

## ACKNOWLEDGMENT

This material is based upon work supported by the Air Force Office of Scientific Research (AFOSR) award numbers LRIR 24RYCOR008 and FA9550-18-1-0355. N. Furman acknowledges partial support from NSF-AFRL Internship Award No. ECCS-2030029. The authors additionally thank R. Marosi, UC Irvine, for contributing to time domain simulations. The authors are thankful to DS SIMULIA for providing CST Studio Suite.

## APPENDIX

We highlight the resilience of SIP features in the dispersion diagram and finite length models to differences in mesh quality in simulations. We focus on the TWG2RA design in this appendix. While we presented the previous eigenmode solver data (the dispersion diagram) using a high-density tetrahedral mesh, we have investigated how reducing the mesh density affects the modal behavior. As the mesh quality is related to resilience of fabrication disorder, this small investigation gives a preliminary estimate of the behavior of on-chip devices.

In Fig. 8(a) we plot the dispersion for the SIP-supporting mode with different mesh qualities. The very low, low, medium, and high quality curves correspond to 2k, 13k, 47k, and over 100k mesh cells, respectively, and the 13k mesh is shown as in inset in the figure. As the quality of the mesh increases, we both see a convergence in the curves along with a flattening of the dispersion diagram expected for the SIP. Remarkably, even with a low-quality mesh, we continue to observe SIP-like properties of the propagating mode. In particular, even the "Very Low" and "Low" quality mesh provide curves that show an SIP-like behavior, though at a frequency that is shifted with respect to the SIP obtained with higher mesh quality, "Medium" and "High" that are both in agreement. These properties facilitate a slowdown of the light (due to the flattening of the dispersion diagram) and suggest initial simulations using a low-quality mesh may provide a good estimate for the dispersion characteristics before undertaking a more computationally demanding high-quality mesh simulation.

We continue this variation of the mesh quality for finite length simulation in Fig. 8(b). Here, we fix the length of the structure to  $N = 50$  unit cells and we present four frequency domain (FD) simulations alongside two time domain (TD) simulations performed using CST Studio Suite. As the TD simulation mesh increases, it agrees more with the FD simulations. And like the eigenmode simulation results, we have very good agreement between the four different FD simulations. Even at a mesh quality ten times worse (dark blue FD 153k curve) compared to the high quality 1.3M mesh cell purple curve, we see very good agreement between the simulations. Further, as the mesh quality degrades, the simulation less accurately represents the physical geometry we are trying to describe. This is analogous to some differences between the simulation geometry and the fabricated devices. In fabrication, many dimensions and properties may change, such as the waveguide width, height, gap size, sidewall angle, or roughness, to name a few. If eigenmode or finite length simulations do not properly reflect these dimensions and properties, like

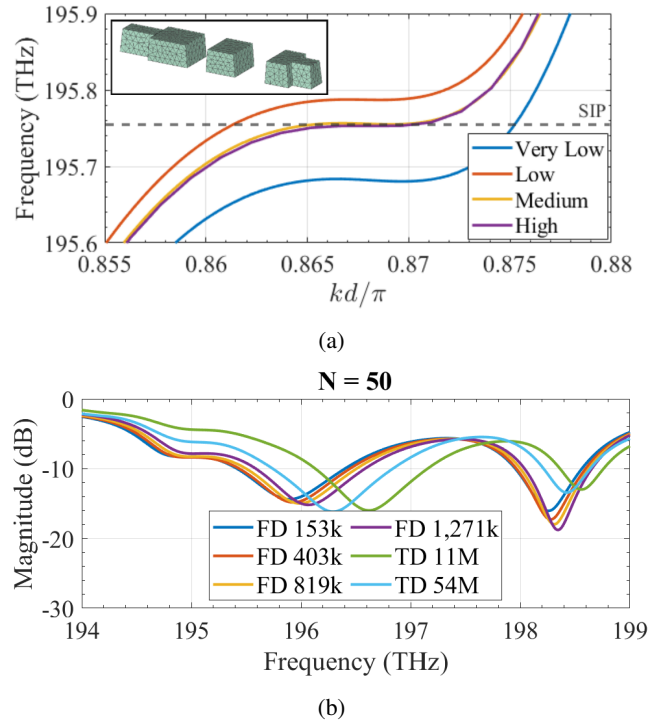


Fig. 8: (a) Dispersion diagram obtained with eigenmode simulation of the TWG2RA design around the SIP (marked by a horizontal line) when varying the mesh quality. The figure inset shows the mesh with low quality (13k mesh cells). (b) Simulated transfer function magnitude for the TWG2RA design with  $N = 50$  unit cells when varying the mesh quality for both frequency domain (FD) and time domain (TD) solvers.

when using a low-quality mesh, we introduce differences between the ‘ideal’ high-quality simulation and the ‘real’ low-quality simulation. With the low-quality simulations still showing SIP-like properties for the design shown in this paper, it is more likely fabricated devices with their disorder are also resilient to waveguide perturbations and will continue to exhibit SIP-like properties.

Not only do these simulations suggest a resilience to some perturbations, so too do these simulations suggest a good quality of the presented simulation results. With a varying mesh quality, we test the convergence of our results and indeed our results do converge to a high degree of accuracy. As mentioned in the prior discussion, we have observed a slight difference in the fabricated devices from simulation models based on other spectrally sensitive devices such as simple ring resonators or such as the waveguides in [31] on the same wafer. Thus, while we spectrally shift the transmission profile to better align simulation and measurements, the various simulation results presented in this appendix still suggest a good resilience to some perturbations.

## REFERENCES

- [1] A. Figotin and I. Vitebskiy, “Electromagnetic unidirectionality in magnetic photonic crystals,” *Physical Review B*, vol. 67, no. 16, p. 165210, 2003.

- [2] —, “Frozen light in photonic crystals with degenerate band edge,” *Physical Review E*, vol. 74, no. 6, 2, p. 066613, 2006.
- [3] —, “Slow wave phenomena in photonic crystals,” *Laser & Photonics Reviews*, vol. 5, no. 2, pp. 201–213, 2011.
- [4] W. Heiss, “Exceptional points of non-hermitian operators,” *J. Phys. A Math. Theor.*, vol. 37, no. 6, pp. 2455–2464, 2004.
- [5] C. E. Rueter, K. G. Makris, R. El-Ganainy, D. N. Christodoulides, M. Segev, and D. Kip, “Observation of parity-time symmetry in optics,” *Nat. Phys.*, vol. 6, no. 3, pp. 192–195, 2010.
- [6] H. Ramezani, T. Kottos, R. El-Ganainy, and D. N. Christodoulides, “Unidirectional nonlinear  $\mathcal{PT}$ -symmetric optical structures,” *Phys. Rev. A*, vol. 82, p. 043803, 2010.
- [7] M. A. K. Othman and F. Capolino, “Theory of exceptional points of degeneracy in uniform coupled waveguides and balance of gain and loss,” *IEEE Trans. Antennas Propag.*, vol. 65, no. 10, pp. 5289–5302, 2017.
- [8] M. Y. Nada, M. A. K. Othman, and F. Capolino, “Theory of coupled resonator optical waveguides exhibiting high-order exceptional points of degeneracy,” *Physical Review B*, vol. 96, no. 18, p. 184304, 2017.
- [9] A. Figotin and I. Vitebskiy, “Gigantic transmission band-edge resonance in periodic stacks of anisotropic layers,” *Physical Review E*, vol. 72, no. 3, 2, p. 036619, 2005.
- [10] —, “Slow light in photonic crystals,” *Waves in Random and Complex Media*, vol. 16, no. 3, pp. 293–382, 2006.
- [11] N. Gutman, W. H. Dupree, Y. Sun, A. A. Sukhorukov, and C. M. de Sterke, “Frozen and broadband slow light in coupled periodic nanowire waveguides,” *Optics Express*, vol. 20, no. 4, pp. 3519–3528, 2012.
- [12] N. Gutman, C. M. de Sterke, A. A. Sukhorukov, and L. C. Botten, “Slow and frozen light in optical waveguides with multiple gratings: Degenerate band edges and stationary inflection points,” *Physical Review A*, vol. 85, no. 3, p. 033804, 2012.
- [13] M. Sumetsky, “Uniform coil optical resonator and waveguide: transmission spectrum, eigenmodes, and dispersion relation,” *Optics Express*, vol. 13, no. 11, pp. 4331–4340, 2005.
- [14] T. Baba and D. Mori, “Slow light engineering in photonic crystals,” *Journal of Physics D: Applied Physics*, vol. 40, no. 9, p. 2659, 2007.
- [15] J. Scheuer and O. Weiss, “The serpentine optical waveguide: engineering the dispersion relations and the stopped light points,” *Optics Express*, vol. 19, no. 12, pp. 11 517–11 528, 2011.
- [16] J. Scheuer and M. Sumetsky, “Optical-fiber microcoil waveguides and resonators and their applications for interferometry and sensing,” *Laser & Photonics Reviews*, vol. 5, no. 4, pp. 465–478, 2011.
- [17] J. R. Burr, N. Gutman, C. M. de Sterke, I. Vitebskiy, and R. M. Reano, “Degenerate band edge resonances in coupled periodic silicon optical waveguides,” *Opt. Express*, vol. 21, no. 7, pp. 8736–8745, 2013.
- [18] B. Paul, K. Sertel, and N. K. Nahar, “Experimental demonstration of frozen-mode enabled slow-wave photonic device in coupled silicon ridge waveguides,” *Journal of Lightwave Technology*, 2024.
- [19] A. Herrero-Parareda, I. Vitebskiy, J. Scheuer, and F. Capolino, “Frozen mode in an asymmetric serpentine optical waveguide,” *Adv. photonics*, vol. 3, no. 9, p. 2100377, 2022.
- [20] B. Paul, N. K. Nahar, and K. Sertel, “Frozen mode in coupled silicon ridge waveguides for optical true time delay applications,” *Journal of the Optical Society of America B - Optical Physics*, vol. 38, no. 5, pp. 1435–1441, 2021.
- [21] B. Paul, K. Sertel, and N. K. Nahar, “Photonic beamforming for 5g and beyond: A review of true time delay devices enabling ultra-wideband beamforming for mmwave communications,” *IEEE Access*, vol. 10, pp. 75 513–75 526, 2022.
- [22] H. Ramezani, S. Kalish, I. Vitebskiy, and T. Kottos, “Unidirectional lasing emerging from frozen light in nonreciprocal cavities,” *Physical review letters*, vol. 112, no. 4, p. 043904, 2014.
- [23] A. Herrero-Parareda, N. Furman, T. Mealy, R. Gibson, R. Bedford, I. Vitebskiy, and F. Capolino, “Lasing at a stationary inflection point,” *Opt. Mater. Express*, vol. 13, no. 5, pp. 1290–1306, 2023.
- [24] N. Furman, A. Herrero-Parareda, I. Vitebskiy, R. Gibson, B. Thompson, R. Bedford, and F. Capolino, “Impact of fabrication disorder on lasing near a stationary inflection point,” *J. Opt. Soc. Am. B*, vol. 42, no. 4, pp. 879–889, 2025.
- [25] K. Zamir-Abramovich, N. Furman, A. Herrero-Parareda, F. Capolino, and J. Scheuer, “Low-threshold lasing with a stationary inflection point in a three-coupled-waveguide structure,” *Physical Review A*, vol. 108, no. 6, p. 063504, 2023.
- [26] N. Furman, T. Mealy, M. S. Islam, I. Vitebskiy, R. Gibson, R. Bedford, O. Boyraz, and F. Capolino, “Frozen mode regime in an optical waveguide with a distributed Bragg reflector,” *Journal of the Optical Society of America B*, vol. 40, no. 5, p. 966, 2023.
- [27] Y. Dattner and O. Yadid-Pecht, “Analysis of the effective refractive index of silicon waveguides through the constructive and destructive interference in a mach-zehnder interferometer,” *IEEE Photonics Journal*, vol. 3, no. 6, pp. 1123–1132, 2011.
- [28] T. Kato, *Perturbation theory for linear operators*. New York: Springer-Verlag New York Inc., 1966, ch. 2.
- [29] N. M. Fahrenkopf, C. McDonough, G. L. Leake, Z. Su, E. Timurdogan, and D. D. Coolbaugh, “The aim photonics mpw: A highly accessible cutting edge technology for rapid prototyping of photonic integrated circuits,” *IEEE Journal of Selected Topics in Quantum Electronics*, vol. 25, no. 5, pp. 1–6, 2019.
- [30] R. Marosi, T. Mealy, A. Figotin, and F. Capolino, “Three-way serpentine slow wave structures with stationary inflection point and enhanced interaction impedance,” *IEEE Transactions on Plasma Science*, vol. 50, no. 12, pp. 4820–4833, 2022.
- [31] N. Furman, A. Herrero-Parareda, A. Rapp, I. Vitebskiy, R. Gibson, B. J. Thompson, D. P. Brown, R. Bedford, and F. Capolino, “Experimental measurement of enhanced group delay silicon photonic waveguides indicative of the frozen mode regime around the stationary inflection point,” *arXiv preprint arXiv:2512.16831*, 2025.